ZESZYT NAUKOWE POLITECHNIKI ŚLĄSKIEJ 2001
Seria: ELEKTRYKA z. 176 Nr kol. 1500

Luděk SCHREIER[1)], Miroslav CHOMÁT[1)], Ivo DOLEŽEL[1)]

EFFECT OF MACHINE GEOMETRY ON HIGHER HARMONICS CONTENT IN AIR-GAP MAGNETIC FIELD OF SYNCHRONOUS RELUCTANCE MACHINE

Summary. The presented paper deals with the effect of rotor geometry on the magnetic field distribution in the air gap. The magnetic field is analysed by means of the finite element method. This method represents, however, quite a laborious and time-consuming process. Therefore, a simpler semi-analytical method for evaluation of the magnetic field distribution in the air gap and following determination of parameters for a numerical model of the machine based on lumped parameters has been proposed. This model enables considering the effect of a series of higher harmonics of the air-gap permeance on electromagnetic quantities of the machine.

Key words: Synchronous reluctance machine, higher harmonic waves

1. INTRODUCTION

Operating properties of AC machines, and of synchronous reluctance machines (SRM's) in particular, are substantially dependent on the field distribution in the air gap. The magnetic field in a SRM is especially influenced by the magnetic rotor saliency. The function of reluctance across the air gap as well as all field quantities in the air gap contain a number of higher spatial harmonics that may substantially distort the waveforms of the phase currents, induced voltages and cause cogging of the electromagnetic torque.

Detailed knowledge of the magnetic field in the machine is vital for development of any reliable and robust control for drives with SRMs. One of suitable models including the higher time and spatial harmonics is based on the space phasor theory. However, many parameters of its equations have to be evaluated from the knowledge of the most significant harmonics of the air gap permeance. Thus, the fundamental problem is to suggest a suitable algorithm for finding their values in an arbitrary operating regime.

An FEM program may be used to calculate the field distribution in the machine and some related quantities. This is, however, generally laborious and time-consuming process, particularly in complex 3D geometries or when taking into account the magnetic saturation. Moreover, the air-gap reluctance or permeance and their harmonic expansions have usually to be determined additionally, beyond the common framework of the field solution. That is why an attempt has been made to develop an alternative method to find the air-gap field distribution and parameters of the dynamic equations.

2. DETERMINATION OF AIR-GAP PERMEANCE

Problems connected with the evaluation of air-gap permeance by traditional methods lead to development of a simpler semianalytical method, whose accuracy is somewhat lower, but the computations are performed at a substantially higher speed. This method enables us to identify the machine parameters from the constructional geometry of the machine and to investigate the effects of higher space harmonics and saturation on the properties of the machine.

The magnetic properties of the air gap are represented by the reluctance functions associated with the stator and rotor. The determination of these functions starts from the profile of the air gap together with stator and rotor slots and saliences. This is based on the assumption that the permeability of iron is much higher than that of vacuum and, therefore, the magnetic field is mainly

[1)] Institute of Electrical Engineering, Academy of Sciences of the Czech Republic, Dolejškova 5, 182 02 Prague 8, Czech Republic. tel.: +420 2 6605 2394, fax.: +420 2 688 3422, e-mail.: {schreier,chomat,dolezel}@iee.cas.cz

affected by the shape of the air gap. The functions are numerically modified to take the effect of non-radial entry of the magnetic flux lines into the iron into consideration. For a particular mutual angular position of the stator and rotor, the function of the resulting reluctance of the machine along the air gap and the waveform of the magnetomotive force along the air gap are evaluated. The application of the Hopkinson law yields the distribution of the magnetic flux density along the air gap from the functions of the reluctance and the magnetomotive force. The effect of the magnetic saturation is introduced by means of an additional reluctance function whose value depends on the magnetic flux density at a particular position.This way a set of non-linear algebraic equations describing the magnetic properties of the machine is obtained. These equations may be numerically solved by means of a suitable iteration method.

The results obtained by the described method for a 3-phase 4-pole SRM (3 stator slots per one pole and phase) with a power output of 0.75 kW have been compared with the results obtained by the FEM. A cross-sectional view of the machine is apparent e.g. from Fig. 1. The axial length of the machine is 98 mm and the rotor slots are skewed. The following paragraphs deal with the analysis of the steady-state operation of the machine in several different modes. First, the machine runs with no mechanical load and the rotor rotates so that its direct axis coincides with the space phasor of the stator current. The stator is supplied with sinusoidal voltage at a frequency of 50 Hz. Second, the machine is mechanically loaded and the load angle is 20 electrical degrees. This corresponds to a lag of 10° in the actual axial cut through the machine. The supply voltage and frequency are the same as in the former case.

When the machine runs at the synchronous speed with sinusoidal stator currents, no currents are induced in the rotor cage by the fundamental spatial harmonic of the current layer in the stator. The eddy currents induced in the rotor slots due to the slot and teeth harmonics are neglected here. The mechanical characteristics of the machine are mainly affected by the distribution of the magnetic flux density in the air gap. The magnetic field distribution in the machine was solved by FEM-based program OPERA (Vector Fields).

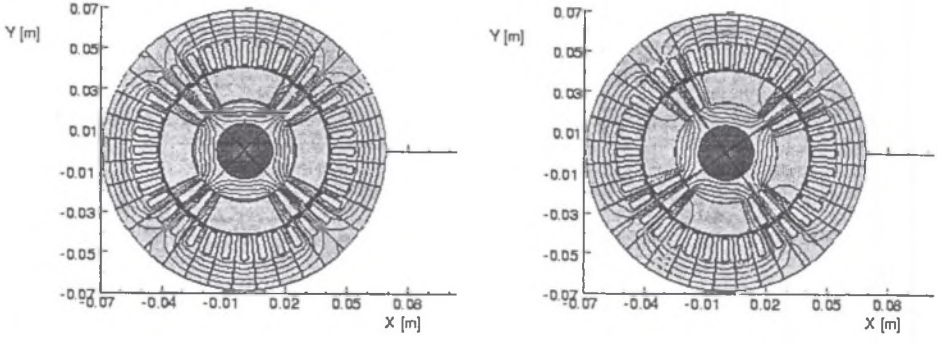

Fig. 1. Field map for J = 2 A/mm^2 :a) α = 0°, b) α = 10°

Figure 1a, b shows the field maps for two different angles (positions), 0° and 10°, between the stator and rotor. The current density in the stator slots is rather low (J = 2 A/mm^2) and the magnetisation of teeth remains in the linear part of the magnetisation curve. The waveforms of the magnetic flux density along the air gap for the same positions are in Fig. 2a, b. From comparison of the two graphs, a relative phase displacement of all the curves against axis d is evident. This is due to the increased load angle of the machine. The agreement between the presented results is very good. Small discrepancies may be brought about by numerical inaccuracies due to discretisation of the thin air gap (FEM) and also due to the way of determination of the additional reluctance function (semianalytical method).

The magnetic flux in selected ferromagnetic parts of the machine such as the stator yoke and the stator teeth was also computed. Figure 3a, b shows the time dependences of the magnetic flux in the stator yoke. In the middle, there are waveforms of the flux flowing through the top part of one stator tooth. The bottom plots show the calculated superposition of the fluxes through three

neighbouring teeth (solid line) and the flux through one pole of the machine across the air gap (dotted line).

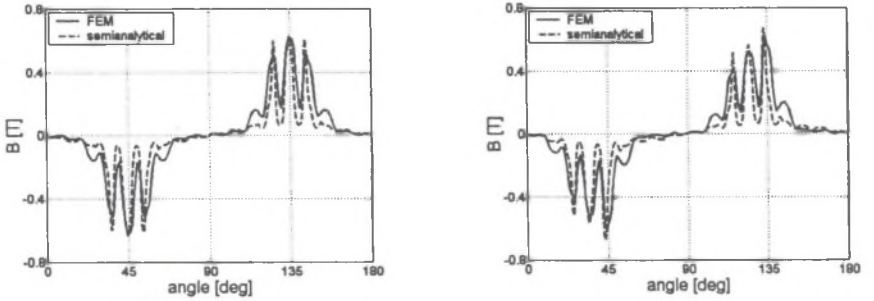

Fig. 2. Magnetic flux density along the air gap for J = 2 A/mm^2: a) α = 0°, b) α = 10°

A number of experiments were carried out in order to verify the results of the described numerical methods. The operating modes that correspond to the modelled ones were investigated. The experimental SRM was equipped with three sensing coils wound around the stator yoke. The angular displacement between these coils was 30°. Additional coils were also placed around four neighbouring stator teeth. This enabled us to monitor simultaneously actual flux in several magnetic paths of the machine.

Figure 4a illustrates the case when the machine is loaded with no mechanical load except for its friction and ventilation losses. The quantities corresponding to those calculated by the numerical models are presented. The waveforms of the magnetic flux in the stator yoke are shown in the top part of the figure. In the middle the waveforms of the magnetic fluxes in the stator teeth are presented. The calculated sum of the three above fluxes is in the bottom picture (solid line). The curve plotted by the dotted line presents the flux across one pole of the machine reconstructed from the measurements of the tooth fluxes. Its magnitude is twice the magnitude measured directly in the yoke. Figure 4b shows the analogous quantities for the loaded machine. The mechanical load was regulated so that a load angle of about 20 electrical degrees was maintained. Figure 5a, b shows the waveforms of the stator phase current and the voltage between the stator winding neutral and the ground.

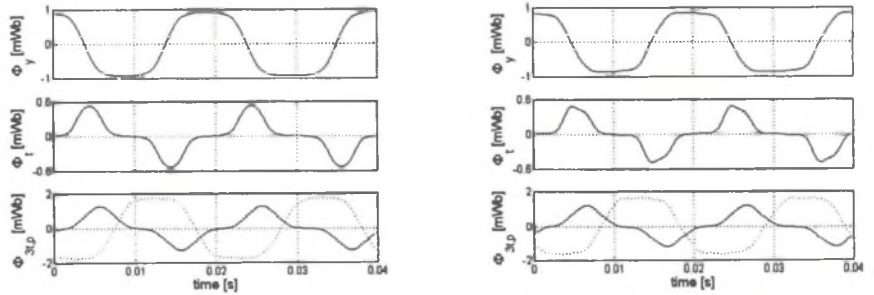

Fig. 3. Magnetic fluxes in the machine obtained by the FEM: a) α = 0°, b) α = 10°

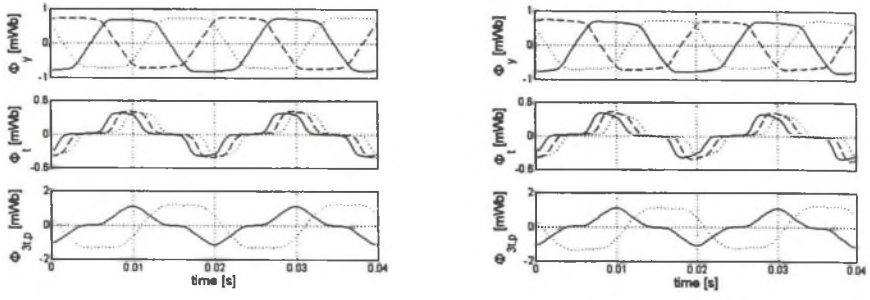

Fig. 4. Measured magnetic fluxes in the machine: a) α = 0°, b) α = 10°

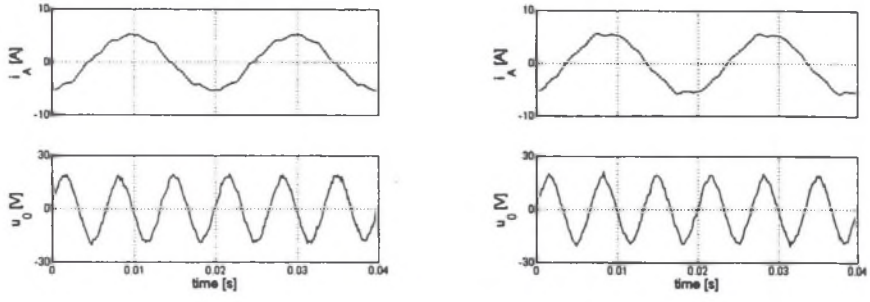

Fig. 5. Measured phase current and the voltage between the stator neutral and the ground: a) α=0°, b) α=10°

3. MATHEMATICAL DESCRIPTION OF SRM WITH CONSIDERATION OF HIGHER HARMONICS OF PERMEANCE OF AIR GAP

The SRM is characterized by a relatively complicated shape of the air-gap. Analysis of the situation in the air-gap may be realized by substitution of its permeance by a series of harmonics [1, 2]. This series may be expressed in the form

$$\lambda(\alpha) = \lambda_0 + \sum_n \lambda_n \cos np(\alpha - \rho - \alpha_n). \tag{1}$$

The series contains constant component λ_0 and harmonic waves with amplitude λ_n. Symbol α is the angle measured from the real axis of the stator reference frame, ρ is the angle between the stator and rotor co-ordinates , p is the number of pole-pairs, and angle α_n determines the position of the maximum of the particular waves. In practice, the value of this angle is either 0 or π/pn.

The influence of stator slots may be respected by a reduction of the constant component. In accordance with [1] and [2], the waves of the magnetic conductivity may be, with advantage, expressed in the form of space phasors. The permeance of the air-gap in position given by angle α is

$$\lambda_n(\alpha) = \mathrm{Re}\left\{\lambda_n e^{jpn(\rho+\alpha_n)}\, e^{-jpn\alpha}\right\}. \tag{2}$$

By analogy, the value of the current layer along the air-gap corresponding to its fundamental wave written by means of the space phasor is

$$A(\alpha) = \frac{1}{p\pi}\mathrm{Re}\left\{i_N e^{-jp\alpha}\right\}. \tag{3}$$

The SRMs are currently produced mostly without winding on the rotor. In this case, the space phasor of machine currents i_N is as follows

$$i_N = N_{S1}\left(i_A + a i_B + i_C a^2\right). \tag{4}$$

Symbol N_{S1} represents the effective number of conductors of one stator phase winding for the fundamental wave, i_A, i_B, i_C are the phase currents and a is

$$a = e^{j2\pi/3}. \tag{5}$$

The expression in brackets in Eq. (4) corresponds to the first symmetrical component of instantaneous values. The symmetrical components are used with advantage in the theory of electrical machines. This definition, for example for stator currents, is

$$i_{S1} = k\left(i_A + i_B a + i_C a^2\right),\ i_{S2} = k\left(i_A + i_B a^2 + i_C a\right),\ i_{S3} = k\left(i_A + i_B + i_C\right). \tag{6}$$

Different authors choose constant k in different ways. The value of $k=2/3$ is frequently used. In [1] and [2] value $k=1/3$ is chosen.

The shape of the flux density in the air-gap as a function of MMF is

$$B(\alpha) = \mu_0 \lambda(\alpha) U_{MMF}(\alpha), \tag{7}$$

$$U_{MMF}(\alpha) = \int_0^{\alpha} A(\xi)\,d\xi + U_{MMF}(0). \tag{8}$$

The substitution for U_{MMF} from Eq. (8) and λ from Eq. (2) into Eq. (7) yields space phasors of fluxes in the yoke of the machine. The rise of these waves of flux is given by an interaction of the wave of MMF and particular waves of magnetic conductivity. In accordance with [2], the flux waves of orders (1+n) and (n-1) rise. These waves expressed in the form of space phasors are

$$\Phi_{(1+n)} = L_{(1+n)} i_N e^{jpn(\rho+\alpha_n)}, \tag{9}$$

$$\Phi_{(n-1)} = -L_{(n-1)} i_N^* e^{jpn(\rho+\alpha_n)} \tag{10}$$

where

$$L_{(1+n)} = \frac{\mu_0 D l \lambda_n}{4\pi p^2 (1+n)} \tag{11}$$

and

$$L_{(n-1)} = \frac{\mu_0 D l \lambda_n}{4\pi p^2 (n-1)}. \tag{12}$$

In these equations, symbol μ_0 represents permeability of vacuum, D is the stator bore, and l is the active length of the machine. Quantities $L_{(1+n)}$ and $L_{(n-1)}$ may be considered as unit inductances indicating relations between current space phasor and the flux components corresponding to the particular waves of magnetic conductivity. The constant component of permeance together with magnetic flux generate flux wave

$$\Phi_{01} = L_0 i_N \tag{13}$$

where

$$L_0 = \frac{\mu_0 D l \lambda_0}{2\pi p^2}. \tag{14}$$

When the second, fourth, and sixth waves of the magnetic conductivity are taken into consideration, the following waves of flux in the yoke rise:

$$\begin{aligned}
\Phi_{11} &= -L_{(2-1)} i_N^* e^{j2p(\rho+\alpha_2)}, \\
\Phi_3 &= L_{(1+2)} i_N e^{j2p(\rho+\alpha_2)} - L_{(4-1)} i_N^* e^{jp4(\rho+\alpha_4)}, \\
\Phi_5 &= L_{(1+4)} i_N e^{j4p(\rho+\alpha_4)} - L_{(6-1)} i_N^* e^{j6p(\rho+\alpha_6)}, \\
\Phi_7 &= L_{(1+6)} i_N e^{j6p(\rho+\alpha_6)}
\end{aligned} \tag{15}$$

where

$$L_{(2-1)} = \frac{\mu_0 Dl\lambda_2}{4\pi p^2},\ L_{(1+2)} = \frac{\mu_0 Dl\lambda_2}{12\pi p^2},\ L_{(4-1)} = \frac{\mu_0 Dl\lambda_4}{12\pi p^2},\ L_{(1+4)} = \frac{\mu_0 Dl\lambda_4}{20\pi p^2},$$

$$L_{(6-1)} = \frac{\mu_0 Dl\lambda_6}{20\pi p^2},\ L_{(1+6)} = \frac{\mu_0 Dl\lambda_6}{28\pi p^2}. \tag{16}$$

The resulting first space phasor of flux is

$$\Phi_1 = \Phi_{01} + \Phi_{11}. \tag{17}$$

The waves of flux of order ν induce into the phase winding voltages

$$u_{Aiv} = N_\nu \mathrm{Re}\left\{\frac{d\Phi_\nu}{dt}\right\},\ u_{Biv} = N_\nu \mathrm{Re}\left\{\frac{d\Phi_\nu}{dt}a^{-\nu}\right\},\ u_{Civ} = N_\nu \mathrm{Re}\left\{\frac{d\Phi_\nu}{dt}a^{-2\nu}\right\} \tag{18}$$

where N_ν is the effective number of turns of one phase for a particular spatial harmonic.

The voltages of the particular phase windings are

$$u_A = R_S i_A + L_{\sigma S}\frac{di_A}{dt} + \sum_\nu N_\nu u_{Aiv},\ u_B = R_S i_B + L_{\sigma S}\frac{di_B}{dt} + \sum_\nu N_\nu u_{Biv},\ u_C = R_S i_C + L_{\sigma S}\frac{di_C}{dt} + \sum_\nu N_\nu u_{Civ} \tag{19}$$

where R_S is the stator resistance and $L_{\sigma S}$ is the leakage inductance.

Substitution of the phase quantities in Eq. (19) by their symmetrical components gives

$$u_{S1} = R_S i_{S1} + L_{\sigma S}\frac{di_{S1}}{dt} + \frac{1}{2}\sum_{\nu=1+3k} N_\nu \frac{d\Phi_\nu}{dt} + \frac{1}{2}\sum_{\nu=2+3k} N_\nu \frac{d\Phi_\nu^*}{dt}, \tag{20}$$

$$u_0 = u_3 = \sum_{\nu=3k} N_\nu \mathrm{Re}\left\{\frac{d\Phi_\nu}{dt}\right\}. \tag{21}$$

The waves of the order $\nu=1+3k$ (where k=0,1, 2, 3...) induce in phase windings voltages of the same sequence as the terminal voltage. The waves of the order $\nu=2+3k$ induce voltages of the reverse sequence, therefore, they occur in Eq. (20) as complex conjugate quantities. The waves of the order $\nu=3k$ induce in all phases identical voltages given by Eq. (21) and do not affect the stator currents, when the stator winding is λ-connected. The substitution of phasors of the flux from Eq. (15) and (17) in to Eq. (20) and (21) gives

$$u_{S1} = \bar{R}_S i_{S1} + \bar{L}_{\sigma S}\frac{di_{S1}}{dt} + \bar{L}_{11}\frac{di_{S1}}{dt} - \bar{L}_{12}\frac{di_{S1}^* e^{j2p(\rho+\alpha_2)}}{dt} + \bar{L}_{51}\frac{di_{S1}^* e^{-j4p(\rho+\alpha_4)}}{dt} - \\ - L_{52}\frac{i_{S1} e^{-j6p(\rho+\alpha_6)}}{dt} + L_{71}\frac{di_{S1} e^{j6p(\rho+\alpha_6)}}{dt}, \tag{22}$$

$$u_0 = \mathrm{Re}\left\{L_{31}\frac{i_{S1} e^{j2p(\rho+\alpha_2)}}{dt} - L_{32}\frac{i_{S1}^* e^{j4p(\rho+\alpha_4)}}{dt}\right\} \tag{23}$$

where

$$L_{11} = \frac{3}{2}N_{S1}N_{S1}L_0,\ L_{12} = \frac{3}{2}N_{S1}N_{S1}L_{(2-1)},\ L_{31} = \frac{3}{2}N_{S1}N_{S3}L_{(1+2)},\ L_{32} = \frac{3}{2}N_{S1}N_{S3}L_{(4-1)},$$

$$L_{51} = \frac{3}{2}N_{S1}N_{S5}L_{(4+1)},\ L_{52} = \frac{3}{2}N_{S1}N_{S5}L_{(6-1)},\ L_{71} = \frac{3}{2}N_{S1}N_{S7}L_{(1+6)}. \tag{24}$$

The more frequently used inductances L_d and L_q in axes d and q of the rotor co-ordinate frame are connected with inductances L_{11}, L_{12} as follows

$$L_d = L_{11} + L_{12}, \tag{25}$$

$$L_q = L_{11} - L_{12}. \tag{26}$$

Because the higher space harmonics of the current layer are not taken into account, only the fundamental space harmonics waves of the current and flux generate the torque in the air-gap. The torque equation may be expressed in the form

$$T = \frac{3}{2}pL_{12}\,\mathrm{Im}\left\{i_{S1}^2 e^{-j2p\rho}\right\}. \tag{27}$$

Constant 3/2 in Eq. (27) corresponds to k=2/3 in Eq. (6). The torque equation is more commonly expressed by means of quantities L_d, L_q,and current components i_{sd} , i_{sq} in rotor co-ordinates. The expression in brackets in Eq. (27) may be rewritten as

$$i_{S1}^2 e^{-j2p\rho} = i_{S\rho}^2 \tag{28}$$

where $i_{s\rho}$ is the symmetrical component of the stator current in the rotor co-ordinates. Hence,

$$T = 3pL_{12}i_{Sd}i_{Sq} . \tag{29}$$

Inductance L_{12} determined from Eqs. (25) and (26) is

$$L_{12} = \frac{1}{2}\left(L_d - L_q\right). \tag{30}$$

The substitution for L_{12} from Eq. (25) into Eq. (26) gives a commonly used expression

$$T = \frac{3}{2}\left(L_d - L_q\right)i_{Sd}i_{Sq} . \tag{31}$$

The transformation of Eqs. (22) and (23) into the rotor co-ordinates has no practical effect because these equations are not formally simplified as in the case when only the fundamental harmonic is considered.

4. EXAMPLES OF NUMERICAL SIMULATION RESULTS

A numerical model based on Eqs. (22) and (23) has been developed. Figure 6 shows the simulated stator voltage, current and voltage in the neutral corresponding to measurements in Fig. 5. The agreement between theoretical and experimental results is very good. Figure 7 depicts the simulated torque in the air gap and instantaneous power defined as

$$P = u_A i_A + u_B i_B + u_C i_C \tag{32}$$

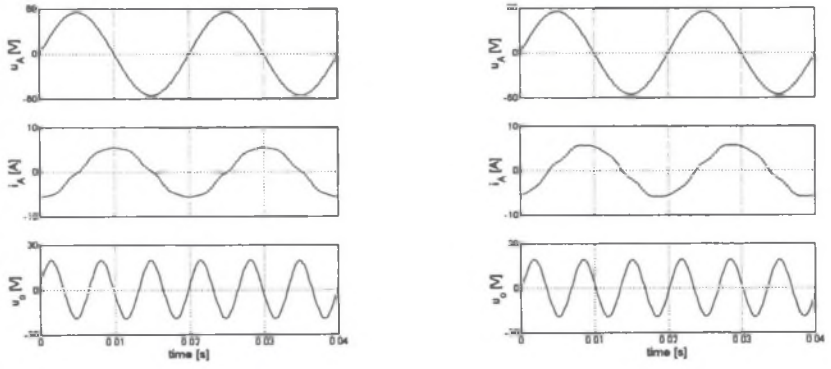

Fig. 6. Simulated phase current and the voltage between the stator neutral and the ground: a) α=0°, b) α=10°

Both torque and power contain alternating components with frequency of the sixth multiple of the supply frequency. The rise of these oscillations is given by interaction of the fundamental time harmonic and the fifth and seventh time harmonic of currents. The time current component corresponding to voltages induced by the fifth space waves of the flux at the synchronous speed rotates clockwise while the fundamental time component rotates counter-clockwise. The speed of the fifth time harmonic is the fifth multiple of the speed of the first one. This results in rise of the oscillation component of the torque and power with the frequency of the sixth multiple of the feeding voltage frequency. The seventh time current component rotates counter-clockwise with speed of the seventh multiple of the fundamental one. This fact results again in rise of oscillations in both torque and power with frequency of the sixth multiple of the terminal voltage frequency.

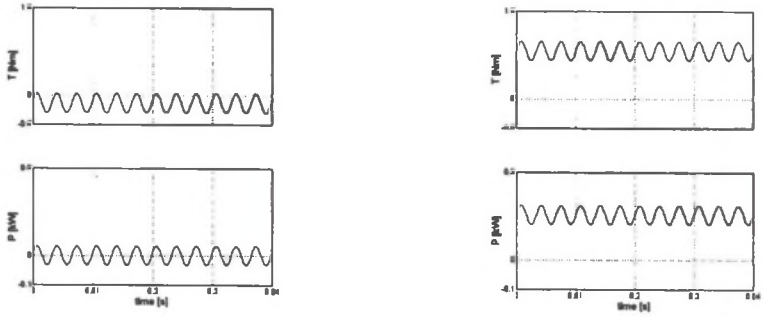

Fig. 7. Simulated torque and power: a) α=0°, b) α=10°

5. CONCLUSION

The proposed mathematical model of a SRM enables detailed investigation of effects of the rotor geometry on electromagnetic quantities in the machine, e.g. currents, torque, power output, which are always distorted by certain content of higher harmonics. Particularly, the currents of the machine are significantly affected even at sinusoidal supply voltage, which results in torque and power output pulsations. The parameters for this model were obtained by means of a relatively simple semi-analytical method. The results were also compared with the results of magnetic field calculation by FEM. The results of the numerical simulation were verified experimentally. There was a good agreement between the theoretical results and the measurement.

REFERENCES

1. Štěpina J.: Symmetrical Components in Rotating Electrical Machines Theory, Prague: Academia, 1969 (in Czech).
2. Štěpina J.: Fundamental Equations of the Space Vector Analysis of Electrical Machines, Acta Technica CSAV, No. 2, 1968, pp. 184-198.

ACKNOWLEDGEMENT

The financial support of the Grant Agency of the Czech Republic, research grant No. 102/01/0181, is acknowledged.

Recenzent: Prof. dr hab. inż. Marian Noga

Wpłynęło do Redakcji dnia 15 marca 2001 r.